

RESEARCH

Open Access



Dynamic nonlinear algebraic models with scale-similarity dynamic procedure for large-eddy simulation of turbulence

Zelong Yuan^{1,2,3}, Yunpeng Wang^{1,2,3}, Chenyue Xie^{1,2,3,4} and Jianchun Wang^{1,2,3*} 

*Correspondence:

wangjc@sustech.edu.cn

¹Department of Mechanics and Aerospace Engineering, Southern University of Science and Technology, Shenzhen 518055 China

²Southern Marine Science and Engineering Guangdong Laboratory (Guangzhou), Guangzhou 511458 China
Full list of author information is available at the end of the article

Abstract

A dynamic nonlinear algebraic model with scale-similarity dynamic procedure (DNAM-SSD) is proposed for subgrid-scale (SGS) stress in large-eddy simulation of turbulence. The model coefficients of the DNAM-SSD model are adaptively calculated through the scale-similarity relation, which greatly simplifies the conventional Germano-identity based dynamic procedure (GID). The *a priori* study shows that the DNAM-SSD model predicts the SGS stress considerably better than the conventional velocity gradient model (VGM), dynamic Smagorinsky model (DSM), dynamic mixed model (DMM) and DNAM-GID model at a variety of filter widths ranging from inertial to viscous ranges. The correlation coefficients of the SGS stress predicted by the DNAM-SSD model can be larger than 95% with the relative errors lower than 30%. In the *a posteriori* testings of LES, the DNAM-SSD model outperforms the implicit LES (ILES), DSM, DMM and DNAM-GID models without increasing computational costs, which only takes up half the time of the DNAM-GID model. The DNAM-SSD model accurately predicts plenty of turbulent statistics and instantaneous spatial structures in reasonable agreement with the filtered DNS data. These results indicate that the current DNAM-SSD model is attractive for the development of highly accurate SGS models for LES of turbulence.

Keywords: Subgrid-scale model, Nonlinear algebraic model, Large-eddy simulation, Incompressible turbulence

1 Introduction

Turbulent flows involve a wide range of length scales across several orders of magnitude, therefore the direct numerical simulation (DNS) of turbulence at high Reynolds number is impractical to solve all flow scales ranging from inertial to viscous ranges [1–3]. Large-eddy simulation (LES) is an effective approach which adopts the coarse mesh to only resolve the large flow scales and model the effect of residual subgrid scales (SGS) on the resolved large scales [4–7]. Extensive SGS models have been proposed to reconstruct the unclosed SGS stress in previous works, including the Smagorinsky model [8–10], the velocity-gradient model (VGM) [11], the scale-similarity model [12, 13], the implicit LES (ILES) [14–16], the Reynolds-stress-constrained LES model [17], the data-driven models [18–25], etc. The Smagorinsky model is one of the commonly-used SGS models

whose model coefficient for the original version is statically adjusted by the experimental and DNS data in the early stage. Germano et al. [26] and Lilly [27] pioneered the development of a dynamical procedure based on the Germano identity through the least-squares algorithm, which makes the parameter of the dynamic Smagorinsky model (DSM) dynamically determined as the flow changes. Subsequently, the dynamical versions of some conventional SGS models with the Germano-identity based dynamic procedure (GID) were proposed [4–7], including the dynamic mixed model (DMM) [28–31], the dynamic Clark model [32], the dynamic localization model [33], etc.

The Smagorinsky model [8, 9, 26, 27] constructs the SGS stress with the linear constitutive relation based on the Boussinesq hypothesis, which requires the alignment between the SGS stress and the filtered strain-rate tensor. Pope [34] derived the general expression between the Reynolds stress and the averaged strain-rate and rotation-rate tensors with eleven integrity basis tensors based on the theory of invariants. Due to the expensive calculations of the high-order basis tensors in the general expression, the numerical verification of Pope's general viscous hypothesis was only limited to the two-dimensional turbulence [34]. Lund and Novikov [35] showed that the sixth invariant can be expressed as the ratio of the other five invariants, and reduced the original eleven polynomial basis tensors to five, which greatly simplified the computational complexity of the nonlinear algebraic SGS model in LES calculations. Especially, the anisotropic part of the SGS stress can be expressed as the general expression of the resolved strain-rate and rotation-rate tensors with five model coefficients [35]. Speziale et al. [36, 37] further simplified Lund's general expression to a quadratic constitutive relation for the Reynolds stress. The model coefficients of the nonlinear algebraic model were mostly determined by the DNS data in the early research work. Wong [38] proposed a two-parameter dynamic nonlinear algebraic model (DNAM) using the quadratic constitutive relation with the Germano-identity based dynamic procedure. Kosović [39] applied the nonlinear constitutive relation to the shear-driven boundary layers at high Reynolds number. Wang et al. [40, 41] proposed a dynamic SGS model based on the quadratic nonlinear constitutive expression with local stability. Marstorp et al. [42] proposed an explicit algebraic SGS stress model with the equilibrium assumptions made on the partial-differential equations of SGS stress, and successfully applied to the rotational channel flow. Recently, a stochastic extension of the explicit algebraic SGS models has been developed by Rasam et al. [43]

In our previous research work, a nonlinear algebraic model based on the artificial neural network (ANN-NAM) was proposed [44], whose model coefficients are predicted by the invariant-input ANN with embedded invariance. The ANN-NAM model [44] reconstructs the SGS stress and statistics of velocity with high accuracy both in the *a priori* and *a posteriori* analyses of LES. Wang et al. [45] proposed an ANN-based semi-explicit spatial gradient model with embedded invariance. A dynamic version of the spatial gradient model (DSGM) [46] was proposed for the parameter determination strategy. Yuan et al. developed deconvolutional artificial neural network (DANN) [21] and dynamic iterative approximate deconvolution (DIAD) models [22] to recover the local unfiltered velocity with the neighboring spatial stencils of the filtered velocity. A scale-similarity-based dynamic procedure (SSD) was proposed to adaptively calculate the weights of the spatial stencil [22]. The DIAD model with the SSD procedure is superior to the other conventional dynamic SGS models in the reconstruction of the statistics of velocity and transient coherent structures of turbulence [22].

The SSD procedure is inspired by the scale-similarity hypothesis [12], assuming that the original unfiltered velocity shares the consistent constitutive relation with the resolved filtered velocity in the inertial region. Bardina et al. [12] developed the scale-similarity model which is formally consistent with the Leonard stress derived by the Germano decomposition [26]. Liu et al. [13] extended the scale-similarity model by introducing the test-level filter. He et al. [47] developed a universal form of Lagrangian velocity correlations at different space separations based on the scale-similarity hypothesis. Stallcup et al. [48, 49] proposed an adaptive scale-similar closure using the generalized representations of the SGS terms by solving a local system identification problem at the test-filter scale. The adaptive scale-similar model can accurately represent the SGS terms near the smallest resolved scales with the minimal tensor representation [48, 49].

In the current research, a novel dynamic nonlinear algebraic model with scale-similarity dynamic procedure (DNAM-SSD) is developed for reconstructing the unclosed SGS stress in LES of incompressible turbulence. The performance of the DNAM-SSD model is examined by comparing with those of some classical SGS models both in the *a priori* and *a posteriori* testings of LES at two filter widths $\bar{\Delta} = 16h_{\text{DNS}}$ and $32h_{\text{DNS}}$ with the corresponding grid resolutions of $N = 128^3$ and 64^3 . The computational accuracy and costs of the newly-proposed scale-similarity based dynamic (SSD) procedure are compared to the conventional Germano-identity based dynamic (GID) procedure. The remainder of the paper is organized as follows. The governing equations of LES will be described in Section 2. The introductions of the conventional SGS models and DNAM models are respectively illustrated in Sections 3 and 4. Section 5 will conduct the numerical simulation of incompressible isotropic turbulence. The *a priori* and *a posteriori* studies are correspondingly provided in Sections 6 and 7. Conclusions are drawn in Section 8.

2 Governing equations of large-eddy simulation

The incompressible turbulence is governed by the Navier-Stokes equations, whose dimensionless conservation form is written as [1]

$$\frac{\partial u_i}{\partial x_i} = 0, \quad (1)$$

$$\frac{\partial u_i}{\partial t} + \frac{\partial (u_i u_j)}{\partial x_j} = -\frac{\partial p}{\partial x_i} + \frac{1}{Re} \frac{\partial^2 u_i}{\partial x_j \partial x_j} + \mathcal{F}_i, \quad (2)$$

where u_i denotes the i -th velocity component ($i = 1, 2, 3$ represents the three directions of the Cartesian coordinate system, respectively), p is the pressure, Re is the Reynolds number, and \mathcal{F}_i is the i -th large-scale force component. [21, 50, 51] For brevity and simplicity, we adopt the summation convention for the repeated indices by default in this paper.

Besides, the governing dimensionless parameter for the incompressible turbulence, namely, the Taylor microscale Reynolds number Re_λ is given by [1]

$$Re_\lambda = \frac{u^{\text{rms}} \lambda}{\sqrt{3} \nu}, \quad (3)$$

where ν denotes the kinematic viscosity and $u^{\text{rms}} = \sqrt{\langle u_i u_i \rangle}$ is the root-mean-square (rms) value of the velocity magnitude. Here, " $\langle \bullet \rangle$ " represents a spatial average over the entire computational domain. In addition, the Taylor microscale λ is expressed as [1]

$$\lambda = u^{\text{rms}} \sqrt{5\nu/\varepsilon}, \quad (4)$$

where $\varepsilon = 2\nu \langle S_{ij}S_{ij} \rangle$ denotes the dissipation rate and $S_{ij} = \frac{1}{2} (\partial u_i/\partial x_j + \partial u_j/\partial x_i)$ is the strain-rate tensor.

For the large-eddy simulation, the resolved large scales are separated from the subgrid small scales by the spatial filtering operation, which is introduced as [1, 2]

$$\bar{f}(\mathbf{x}) = \int_{\Omega} f(\mathbf{x} - \mathbf{r}) G(\mathbf{r}; \bar{\Delta}) d\mathbf{r}, \tag{5}$$

where $f(\mathbf{x})$ represents the arbitrary physical variable, and an overbar stands for the low-pass spatial filtering. Here, Ω denotes the entire physical domain, with G and $\bar{\Delta}$ respectively being the spatial filter function and filter width. The governing equations for the LES can be obtained by applying the spatial filtering on the Eqs. (1) and (2), correspondingly, which can be derived as [1, 2]

$$\frac{\partial \bar{u}_i}{\partial x_i} = 0, \tag{6}$$

$$\frac{\partial \bar{u}_i}{\partial t} + \frac{\partial (\bar{u}_i \bar{u}_j)}{\partial x_j} = -\frac{\partial \bar{p}}{\partial x_i} - \frac{\partial \tau_{ij}}{\partial x_j} + \frac{1}{Re} \frac{\partial^2 \bar{u}_i}{\partial x_j \partial x_j} + \bar{f}_i. \tag{7}$$

Here, the unclosed SGS stress τ_{ij} in the Eq. (7) is defined by [4–6]

$$\tau_{ij} = \overline{u_i u_j} - \bar{u}_i \bar{u}_j. \tag{8}$$

The SGS stress involves the nonlinear interactions between the resolved large scales and under-solved small scales, therefore additional SGS stress modeling is required to close the governing equations of LES. In the following two sections, the conventional SGS models and the proposed dynamic nonlinear algebraic models with scale-similarity dynamic procedure (SSD) are respectively described for the LES computations.

3 Conventional SGS models

The explicit modeling for the unclosed SGS stress can be divided into the functional modeling and structural modeling. The functional models mimic the forward energy transfer from the resolved large scales to the residual small scales by constructing the explicit eddy-viscosity forms, while the structural modeling is established by the truncated series expansions or the hypothesis of scale similarity to correctly recover the SGS stress with high accuracy. A typical functional model is the dynamic Smagorinsky model (DSM), whose constitutive relation for the deviatoric SGS stress is given by [26, 27]

$$\tau_{ij}^A = \tau_{ij} - \frac{\delta_{ij}}{3} \tau_{kk} = -2C_S^2 \bar{\Delta}^2 |\bar{S}| \bar{S}_{ij}, \tag{9}$$

where $|\bar{S}| = (2\bar{S}_{ij}\bar{S}_{ij})^{1/2}$ is the characteristic filtered strain rate, and $\bar{S}_{ij} = \frac{1}{2} (\partial \bar{u}_i/\partial x_j + \partial \bar{u}_j/\partial x_i)$ is the filtered strain-rate tensor. The superscript ‘‘A’’ represents the trace-free part of the arbitrary variables, namely, $(\bullet)_{ij}^A = (\bullet)_{ij} - (\bullet)_{kk} \delta_{ij}/3$. Here, the isotropic SGS stress τ_{kk} is absorbed into the pressure term. C_S^2 is the Smagorinsky coefficient, which can be determined by the Germano identity dynamic procedure (GID). The test-filter level SGS stress with the double-filtering scale $\bar{\bar{\Delta}} = 2\bar{\Delta}$ is expressed as [26, 27]

$$\bar{\tau}_{ij} = \widetilde{\overline{u_i u_j}} - \bar{\bar{u}}_i \bar{\bar{u}}_j, \tag{10}$$

where a tilde stands for the test filtering operation at the filter scale $\tilde{\Delta}$. The deviatoric part of \mathcal{T}_{ij} can be modeled based on the scale-invariance hypothesis, defined by [26, 27]

$$\mathcal{T}_{ij}^A = \mathcal{T}_{ij} - \frac{\delta_{ij}}{3} \mathcal{T}_{kk} = -2C_S^2 \tilde{\Delta}^2 \left| \tilde{S} \right| \tilde{S}_{ij}. \tag{11}$$

These two SGS stresses with different filter scales, namely, τ_{ij} and \mathcal{T}_{ij} satisfy the Germano identity, expressed as [26]

$$\mathcal{L}_{ij} = \mathcal{T}_{ij} - \tilde{\tau}_{ij} = \widetilde{\tilde{u}_i \tilde{u}_j} - \tilde{u}_i \tilde{u}_j, \tag{12}$$

where the Leonard stress \mathcal{L}_{ij} can be calculated using the resolved filtered field for LES calculations. Therefore, the optimal Smagorinsky coefficient C_S^2 can be further determined by the least-squares algorithm, namely [27]

$$C_S^2 = \frac{\langle \mathcal{L}_{ij}^A \mathcal{M}_{ij} \rangle}{\langle \mathcal{M}_{kl} \mathcal{M}_{kl} \rangle}, \tag{13}$$

where $\mathcal{L}_{ij}^A = \mathcal{L}_{ij} - \frac{1}{3} \delta_{ij} \mathcal{L}_{kk}$, and $\mathcal{M}_{ij} = \tilde{\alpha}_{ij} - \beta_{ij}$. Here $\alpha_{ij} = 2\bar{\Delta}^2 |\bar{S}| \bar{S}_{ij}$, $\beta_{ij} = 2\tilde{\Delta}^2 |\tilde{S}| \tilde{S}_{ij}$.

A typical structural model is the velocity gradient model (VGM) based on the truncated Taylor series expansions, given by [11]

$$\tau_{ij} = \frac{\bar{\Delta}^2}{12} \frac{\partial \bar{u}_i}{\partial x_k} \frac{\partial \bar{u}_j}{\partial x_k}. \tag{14}$$

The dynamic mixed model (DMM) combines the scale-similarity model with the dissipative Smagorinsky term, which can overcome the deficiency of numerical instability in the structural modeling of the SGS stress. The SGS stresses constructed by the DMM model at scales $\bar{\Delta}$ and $\tilde{\Delta}$ are expressed, respectively, as [12, 28, 52]

$$\tau_{ij} = C_1 h_{1,ij} + C_2 h_{2,ij}, \tag{15}$$

$$\mathcal{T}_{ij} = C_1 H_{1,ij} + C_2 H_{2,ij}, \tag{16}$$

where $h_{1,ij} = -2\bar{\Delta}^2 |\bar{S}| \bar{S}_{ij}$, $h_{2,ij} = \widetilde{\tilde{u}_i \tilde{u}_j} - \tilde{u}_i \tilde{u}_j$, $H_{1,ij} = -2\tilde{\Delta}^2 |\tilde{S}| \tilde{S}_{ij}$, and $H_{2,ij} = \widehat{\tilde{u}_i \tilde{u}_j} - \hat{\tilde{u}}_i \hat{\tilde{u}}_j$. Here, the hat stands for the test filtering at scale $\hat{\Delta} = 4\bar{\Delta}$. Similar to the DSM model, the model coefficients C_1 and C_2 are calculated by the Germano identity dynamic procedure, namely [21, 22]

$$C_1 = \frac{\langle N_{ij}^2 \rangle \langle \mathcal{L}_{ij} M_{ij} \rangle - \langle M_{ij} N_{ij} \rangle \langle \mathcal{L}_{ij} N_{ij} \rangle}{\langle N_{ij}^2 \rangle \langle M_{ij}^2 \rangle - \langle M_{ij} N_{ij} \rangle^2}, \tag{17}$$

$$C_2 = \frac{\langle M_{ij}^2 \rangle \langle \mathcal{L}_{ij} N_{ij} \rangle - \langle M_{ij} N_{ij} \rangle \langle \mathcal{L}_{ij} M_{ij} \rangle}{\langle N_{ij}^2 \rangle \langle M_{ij}^2 \rangle - \langle M_{ij} N_{ij} \rangle^2}, \tag{18}$$

where $M_{ij} = H_{1,ij} - \tilde{h}_{1,ij}$, and $N_{ij} = H_{2,ij} - \tilde{h}_{2,ij}$.

4 Dynamic nonlinear algebraic models (DNAM)

In the SGS stress modeling, the constitutive relation of the unclosed SGS stress can be regarded as the function of the local filtered quantities, i.e., the filtered strain-rate tensor \bar{S}_{ij} and filtered rotation-rate tensor $\bar{\Omega}_{ij}$, namely [34, 35]

$$\tau_{ij} = f(\bar{S}_{ij}, \bar{\Omega}_{ij}; \delta_{ij}, \bar{\Delta}), \tag{19}$$

where the filtered rotation-rate tensor $\bar{\Omega}_{ij} = \frac{1}{2} (\partial \bar{u}_i / \partial x_j - \partial \bar{u}_j / \partial x_i)$. For brevity and simplicity of the tensorial polynomials, the matrix multiplications for the tensor contractions are expressed as [34, 35, 40]

$$\bar{S}^2 = \bar{S}_{ik} \bar{S}_{kj}, \quad \bar{S} \bar{\Omega} = \bar{S}_{ik} \bar{\Omega}_{kj}, \quad tr(\bar{S} \bar{\Omega}^2) = \bar{S}_{ij} \bar{\Omega}_{jk} \bar{\Omega}_{ki}. \tag{20}$$

A general expression of the modeled SGS stress [Eq. (19)] can be expanded to the sum of an infinite number of tensorial polynomials with the form $\bar{S}^{m_1} \bar{\Omega}^{n_1} \bar{S}^{m_2} \bar{\Omega}^{n_2} \dots$, where m_i and n_i are positive integers. The infinite tensorial polynomials can be reduced to a finite number by the Cayley-Hamilton theorem [34, 35, 40], thus the modeled SGS stress can be expressed as the linear combination of the basis tensors formed by the product of \bar{S} and $\bar{\Omega}$, namely [34]

$$\tau_{ij} = \sum_{n=1}^{11} g_n(\lambda_1, \lambda_2, \dots, \lambda_6) T_{ij}^{(n)}, \tag{21}$$

where $T_{ij}^{(n)}$ is the n -th basis tensor and the model coefficients g_n are functions of the six integrity invariants λ_m ($m = 1, 2, \dots, 6$). Here, the eleven basis tensors $T_{ij}^{(n)}$ and six independent invariants λ_m are respectively expressed as [34]

$$\begin{aligned} \mathbf{T}^{(1)} &= \bar{S}, & \mathbf{T}^{(2)} &= \bar{S}^2, \\ \mathbf{T}^{(3)} &= \bar{\Omega}^2, & \mathbf{T}^{(4)} &= \bar{S} \bar{\Omega} - \bar{\Omega} \bar{S}, \\ \mathbf{T}^{(5)} &= \bar{S}^2 \bar{\Omega} - \bar{\Omega} \bar{S}^2, & \mathbf{T}^{(6)} &= \mathbf{I}, \\ \mathbf{T}^{(7)} &= \bar{S} \bar{\Omega}^2 + \bar{\Omega}^2 \bar{S}, & \mathbf{T}^{(8)} &= \bar{\Omega} \bar{S} \bar{\Omega}^2 - \bar{\Omega}^2 \bar{S} \bar{\Omega}, \\ \mathbf{T}^{(9)} &= \bar{S} \bar{\Omega} \bar{S}^2 - \bar{S}^2 \bar{\Omega} \bar{S}, & \mathbf{T}^{(10)} &= \bar{S}^2 \bar{\Omega}^2 + \bar{\Omega}^2 \bar{S}^2, \\ \mathbf{T}^{(11)} &= \bar{\Omega} \bar{S}^2 \bar{\Omega}^2 - \bar{\Omega}^2 \bar{S}^2 \bar{\Omega}, \end{aligned} \tag{22}$$

$$\begin{aligned} \lambda_1 &= tr(\bar{S}^2), & \lambda_2 &= tr(\bar{\Omega}^2), \\ \lambda_3 &= tr(\bar{S}^3), & \lambda_4 &= tr(\bar{S} \bar{\Omega}^2), \\ \lambda_5 &= tr(\bar{S}^2 \bar{\Omega}^2), & \lambda_6 &= tr(\bar{S}^2 \bar{\Omega}^2 \bar{S} \bar{\Omega}). \end{aligned} \tag{23}$$

If the model coefficients g_n are relaxed as the ratios of polynomials of these integrity invariants, the number of the above basis tensors can be reduced from eleven to five. In accordance with the dimensional consistency, the anisotropic part of the modeled SGS stress can be given by [35]

$$\begin{aligned} \tau_{ij}^A &= \bar{\Delta}^2 \sum_{n=1}^5 C_n \mathbb{T}_{ij}^{(n),A} \\ &= \bar{\Delta}^2 \left[C_1 |\bar{S}| \bar{S} + C_2 (\bar{S}^2)^A + C_3 (\bar{\Omega}^2)^A + C_4 (\bar{S} \bar{\Omega} - \bar{\Omega} \bar{S}) + \frac{C_5}{|\bar{S}|} (\bar{S}^2 \bar{\Omega} - \bar{\Omega} \bar{S}^2) \right], \end{aligned} \tag{24}$$

where the characteristic filtered strain rate $|\bar{S}| = (2\bar{S}_{ij}\bar{S}_{ij})^{1/2}$, and C_n are five dimensionless model coefficients. The corresponding basis tensors $\mathbb{T}_{ij}^{(n)}$ that satisfy the consistent dimension with the square of the velocity gradient are defined by

$$\mathbb{T}_{ij}^{(1)} = |\bar{S}| \bar{S}, \quad \mathbb{T}_{ij}^{(2)} = \bar{S}^2, \quad \mathbb{T}_{ij}^{(3)} = \bar{\Omega}^2, \quad \mathbb{T}_{ij}^{(4)} = \bar{S} \bar{\Omega} - \bar{\Omega} \bar{S}, \quad \mathbb{T}_{ij}^{(5)} = \frac{1}{|\bar{S}|} (\bar{S}^2 \bar{\Omega} - \bar{\Omega} \bar{S}^2). \tag{25}$$

In the paper, two dynamic procedures are adopted to determine the model coefficients C_n of the dynamic nonlinear algebraic models (DNAM). One is the Germano identity

dynamic (GID) procedure based on the scale-invariance assumption, and the other is the newly proposed scale-similarity dynamic (SSD) procedure in accordance with the scale-similarity relation. The rest of this section will be divided into two subsections to respectively introduce these two different modeling approaches.

4.1 DNAM models with Germano identity dynamic procedure (DNAM-GID)

Similar to the conventional dynamic SGS models (e.g. DSM and DMM models), the DNAM model with Germano identity dynamic procedure, abbreviated as DNAM-GID, introduces the test-filter level SGS stress \mathcal{T}_{ij} at the double-filtering scale $\tilde{\Delta} = 2\bar{\Delta}$, modeled by

$$\begin{aligned} \mathcal{T}_{ij}^A &= \tilde{\Delta}^2 \sum_{n=1}^5 C_n \mathbb{H}_{ij}^{(n),A} \\ &= \tilde{\Delta}^2 \left[C_1 |\tilde{\mathbf{S}}| \tilde{\mathbf{S}} + C_2 (\tilde{\mathbf{S}}^2)^A + C_3 (\tilde{\tilde{\Omega}}^2)^A + C_4 (\tilde{\mathbf{S}}\tilde{\tilde{\Omega}} - \tilde{\tilde{\Omega}}\tilde{\mathbf{S}}) + \frac{C_5}{|\tilde{\mathbf{S}}|} (\tilde{\mathbf{S}}^2 \tilde{\tilde{\Omega}} - \tilde{\tilde{\Omega}} \tilde{\mathbf{S}}^2) \right]. \end{aligned} \tag{26}$$

Here, $\mathbb{H}_{ij}^{(n)}$ is the n -th basis tensor at the test filter scale $\tilde{\Delta} = 2\bar{\Delta}$, expressed as

$$\mathbb{H}_{ij}^{(1)} = |\tilde{\mathbf{S}}| \tilde{\mathbf{S}}, \mathbb{H}_{ij}^{(2)} = \tilde{\mathbf{S}}^2, \mathbb{H}_{ij}^{(3)} = \tilde{\tilde{\Omega}}^2, \mathbb{H}_{ij}^{(4)} = \tilde{\mathbf{S}}\tilde{\tilde{\Omega}} - \tilde{\tilde{\Omega}}\tilde{\mathbf{S}}, \mathbb{H}_{ij}^{(5)} = \frac{1}{|\tilde{\mathbf{S}}|} (\tilde{\mathbf{S}}^2 \tilde{\tilde{\Omega}} - \tilde{\tilde{\Omega}} \tilde{\mathbf{S}}^2). \tag{27}$$

Consistent with Eq. (12), the modeled SGS stresses τ_{ij} and \mathcal{T}_{ij} at different filter scales satisfy the Germano identity, namely

$$\mathcal{L}_{ij}^A = \mathcal{T}_{ij}^A - \tilde{\tau}_{ij}^A = \sum_{n=1}^5 C_n \mathbb{M}_{ij}^{(n)}, \tag{28}$$

where $\mathbb{M}_{ij}^{(n)} = \tilde{\Delta}^2 \mathbb{H}_{ij}^{(n),A} - \bar{\Delta}^2 \tilde{\mathbb{T}}_{ij}^{(n),A}$. The model coefficients C_n can be further calculated by the least-squares algorithm, derived by

$$\sum_{m=1}^5 C_m \langle \mathbb{M}_{ij}^{(m)} \mathbb{M}_{ij}^{(n)} \rangle = \langle \mathcal{L}_{ij}^A \mathbb{M}_{ij}^{(n)} \rangle, \quad (n = 1, 2, \dots, 5). \tag{29}$$

For the DNAM-GID model, the optimal model coefficients C_n can be obtained by solving the system of five linear equations in Eq. (29).

4.2 DNAM models with scale-similarity dynamic procedure (DNAM-SSD)

In this paper, we propose a novel scale-similarity dynamic procedure for the DNAM model to determine the optimal model coefficients dynamically. The real SGS stress can be regarded as the nonlinear function of the velocity u_i and the filter kernel at scale $\bar{\Delta}$, whereas the SGS stress modeled by the DNAM model has the nonlinear constitutive relation with the local filtered physical quantities (e.g. the filtered strain-rate and rotation-rate tensors $\tilde{\mathbf{S}}$ and $\tilde{\tilde{\Omega}}$),

$$\begin{aligned} \tau_{ij}^A &= \tau_{ij}^A(u_i; \bar{\Delta}) = (\overline{u_i u_j} - \bar{u}_i \bar{u}_j)^A = \sum_{n=1}^5 C_n \mathbb{T}_{ij}^{(n),A}(\bar{\mathbf{S}}, \bar{\Omega}) \\ &= \bar{\Delta}^2 \left[C_1 |\bar{\mathbf{S}}| \bar{\mathbf{S}} + C_2 (\bar{\mathbf{S}}^2)^A + C_3 (\bar{\Omega}^2)^A + C_4 (\bar{\mathbf{S}} \bar{\Omega} - \bar{\Omega} \bar{\mathbf{S}}) + \frac{C_5}{|\bar{\mathbf{S}}|} (\bar{\mathbf{S}}^2 \bar{\Omega} - \bar{\Omega} \bar{\mathbf{S}}^2) \right]. \end{aligned} \tag{30}$$

Based on the scale-similarity hypothesis, the modeled SGS stress at the filter scale $\tilde{\Delta}$ shares the consistent model coefficients C_n with that at the filter scale $\bar{\Delta}$, namely

$$\begin{aligned} \tau_{ij}^A(u_i; \tilde{\Delta}) &= (\widetilde{u_i u_j} - \tilde{u}_i \tilde{u}_j)^A = \sum_{n=1}^5 C_n \mathbb{T}_{ij}^{(n),A}(\tilde{\mathbf{S}}, \tilde{\Omega}) \\ &= \tilde{\Delta}^2 \left[C_1 |\tilde{\mathbf{S}}| \tilde{\mathbf{S}} + C_2 (\tilde{\mathbf{S}}^2)^A + C_3 (\tilde{\Omega}^2)^A + C_4 (\tilde{\mathbf{S}} \tilde{\Omega} - \tilde{\Omega} \tilde{\mathbf{S}}) + \frac{C_5}{|\tilde{\mathbf{S}}|} (\tilde{\mathbf{S}}^2 \tilde{\Omega} - \tilde{\Omega} \tilde{\mathbf{S}}^2) \right]. \end{aligned} \tag{31}$$

The constitutive equation of the SGS stress is assumed to be invariant to the physical field, therefore we can replace the unfiltered velocity u_i with the filtered velocity \bar{u}_i in Eq. (31) and obtain

$$\begin{aligned} \mathcal{L}_{ij}^A &= \tau_{ij}^A(\bar{u}_i; \tilde{\Delta}) = (\widetilde{\bar{u}_i \bar{u}_j} - \tilde{\bar{u}}_i \tilde{\bar{u}}_j)^A = \sum_{n=1}^5 C_n \mathbb{T}_{ij}^{(n),A}(\tilde{\tilde{\mathbf{S}}}, \tilde{\tilde{\Omega}}) \\ &= \tilde{\Delta}^2 \left[C_1 |\tilde{\tilde{\mathbf{S}}}| \tilde{\tilde{\mathbf{S}}} + C_2 (\tilde{\tilde{\mathbf{S}}}^2)^A + C_3 (\tilde{\tilde{\Omega}}^2)^A + C_4 (\tilde{\tilde{\mathbf{S}}} \tilde{\tilde{\Omega}} - \tilde{\tilde{\Omega}} \tilde{\tilde{\mathbf{S}}}) + \frac{C_5}{|\tilde{\tilde{\mathbf{S}}}|} (\tilde{\tilde{\mathbf{S}}}^2 \tilde{\tilde{\Omega}} - \tilde{\tilde{\Omega}} \tilde{\tilde{\mathbf{S}}}^2) \right]. \end{aligned} \tag{32}$$

\mathcal{L}_{ij}^A is the anisotropic part of the resolved Leonard stress. For simplicity, we let $\mathbb{N}_{ij}^{(n)} = \mathbb{T}_{ij}^{(n),A}(\tilde{\tilde{\mathbf{S}}}, \tilde{\tilde{\Omega}})$ and Eq. (32) is abbreviated as $\mathcal{L}_{ij}^A = \sum_{n=1}^5 C_n \mathbb{N}_{ij}^{(n)}$. Since \mathcal{L}_{ij}^A and $\mathbb{N}_{ij}^{(n)}$ are both resolved in the filtered field, the model coefficients C_n can be determined by the least-squares method,

$$\sum_{m=1}^5 C_m \langle \mathbb{N}_{ij}^{(m)} \mathbb{N}_{ij}^{(n)} \rangle = \langle \mathcal{L}_{ij}^A \mathbb{N}_{ij}^{(n)} \rangle, \quad (n = 1, 2, \dots, 5). \tag{33}$$

It is worth noting that the DNAM-SSD model only calculates $\mathbb{T}_{ij}^{(n),A}(\bar{\mathbf{S}}, \bar{\Omega})$ and $\mathbb{T}_{ij}^{(n),A}(\tilde{\tilde{\mathbf{S}}}, \tilde{\tilde{\Omega}})$ rather than $\mathbb{T}_{ij}^{(n),A}(\bar{\mathbf{S}}, \tilde{\tilde{\Omega}})$, $\mathbb{T}_{ij}^{(n),A}(\tilde{\tilde{\mathbf{S}}}, \bar{\Omega})$ and $\tilde{\mathbb{T}}_{ij}^{(n),A}(\bar{\mathbf{S}}, \bar{\Omega})$ in the DNAM-GID model, therefore the scale-similarity dynamic procedure simplifies the conventional dynamic procedure based on the Germano identity. Besides, in the following sections, we can show that the DNAM model with the proposed scale-similarity dynamic procedure performs better than that with the conventional GID procedure both in the *a priori* and the *a posteriori* testings of incompressible turbulence.

5 Numerical simulation of incompressible isotropic turbulence

In order to validate the performance of the proposed DNAM-SSD model, the numerical simulation of incompressible isotropic turbulence is performed in a cubic box of $(2\pi)^3$ with periodic boundary conditions at the Taylor Reynolds number $Re_\lambda \approx 250$.

The pseudo-spectral approach with the two-thirds dealiasing rule is adopted for the spatial discretization of the governing equation. A second-order explicit Adams-Bashforth scheme [53] is applied to the time advancement. The large-scale forcing is implemented on the two lowest wavenumber shells [21, 50, 51] to keep the turbulence in equilibrium. In the paper, we use $N = 1024^3$ uniform grids in the DNS calculation with the grid spacing $h_{DNS} = 2\pi/1024$. The kinematic viscosity is set to $\nu = 1/Re = 0.001$. The detailed one-point statistics of DNS calculation are summarized in Table 1. Here, $k_{max} = \frac{2\pi}{3h_{DNS}}$ represents the largest effective wavenumber after the fully two-thirds dealiasing, and $\omega^{rms} = \sqrt{\langle \omega_i \omega_i \rangle}$ stands for the root-mean-square value of the vorticity magnitude, where $\omega = \nabla \times \mathbf{u}$ represents the vorticity which is the curl of the velocity field. The Kolmogorov length scale η and the integral length scale L_I represent the smallest resolved scale and the largest characteristic scale, which are defined, respectively, by

$$\eta = \left(\frac{\nu^3}{\varepsilon} \right)^{1/4}, \tag{34}$$

$$L_I = \frac{3\pi}{2(u^{rms})^2} \int_0^{+\infty} \frac{E(k)}{k} dk, \tag{35}$$

where $\varepsilon = 2\nu \langle S_{ij} S_{ij} \rangle$ is the dissipation rate. The total turbulent kinetic energy $E_k = \frac{1}{2} \langle u_i u_i \rangle = \int_0^{+\infty} E(k) dk$, and $E(k)$ stands for the velocity spectrum. The resolution parameter $k_{max}\eta \geq 2.1$ is found to be sufficient enough for the convergence of turbulent kinetic energy at all scales [54, 55].

In the paper, the filtered physical quantities and the real SGS stress τ_{ij} are calculated using a Gaussian filter, which is expressed as [1, 2]

$$G(\mathbf{r}; \bar{\Delta}) = \left(\frac{6}{\pi \bar{\Delta}^2} \right)^{1/2} \exp\left(-\frac{6\mathbf{r}^2}{\bar{\Delta}^2}\right). \tag{36}$$

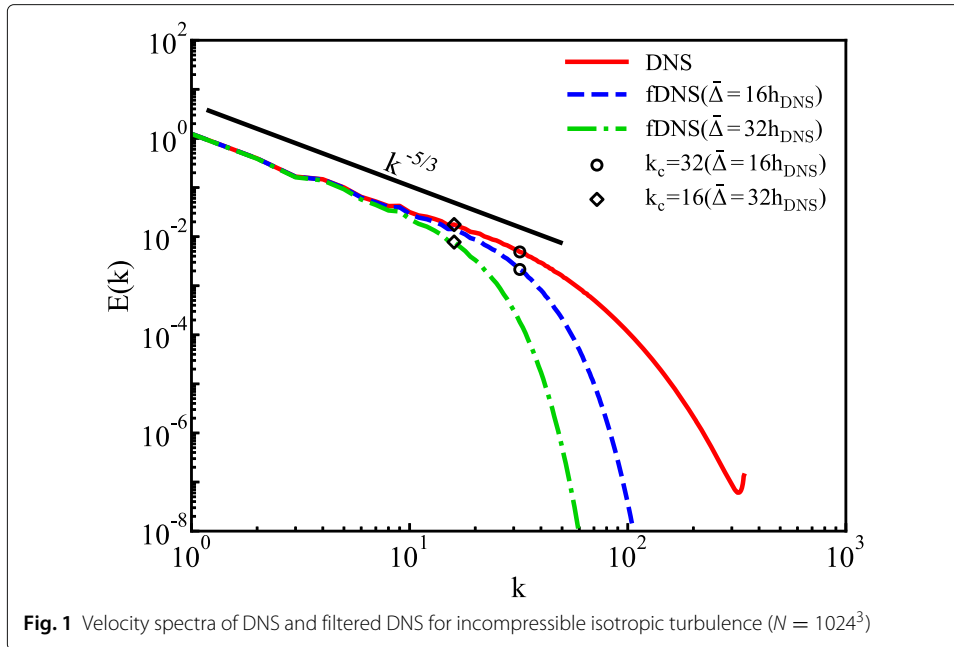
We select two filter scales ($\bar{\Delta} = 16h_{DNS}$ and $32h_{DNS}$) for model verification, and the corresponding cutoff wavenumbers are $k_c = \pi/\bar{\Delta} = 32$ and 16, respectively. Figure 1 shows the velocity spectra of the DNS and filtered DNS at both filter widths ($\bar{\Delta} = 16h_{DNS}$ and $32h_{DNS}$). The filtered velocity spectra almost overlap with the DNS data at the low-wavenumber region satisfying the Kolmogorov $k^{-5/3}$ scaling, while generally diminish with the increasing of wavenumbers, and drop rapidly at the region larger than the truncated wavenumber k_c . More kinetic energy is filtered out at a larger filter scale, therefore the filtered velocity spectrum at $\bar{\Delta} = 32h_{DNS}$ is lower than that at $\bar{\Delta} = 16h_{DNS}$. Overall 95% and 88% of the turbulent kinetic energy is retained in the filtered velocity field at the filter widths $\bar{\Delta} = 16h_{DNS}$ and $32h_{DNS}$, respectively.

6 A priori study of the DNAM models

In the *a priori* analysis, twenty snapshots of DNS data at equal temporal intervals during two large-eddy turnover periods ($\tau = L_I/u^{rms}$) are adopted to examine the model accuracy of the DNAM-GID and DNAM-SSD models with several filter scales ranging from

Table 1 One-point statistics for the DNS with grid resolution of 1024^3

Re_λ	E_k	$k_{max}\eta$	η/h_{DNS}	L_I/η	λ/η	u^{rms}	ω^{rms}	ε
252	2.63	2.11	1.01	235.2	31.2	2.30	26.90	0.73



$\bar{\Delta} = 4h_{\text{DNS}}$ to $\bar{\Delta} = 64h_{\text{DNS}}$. Two evaluation metrics are used to quantify the distinction between the real value (Q^{real}) and the modeled value (Q^{model}) for targeted variable Q , namely the correlation coefficient $C(Q)$ and the relative error $E_r(Q)$, respectively defined by [21, 22]

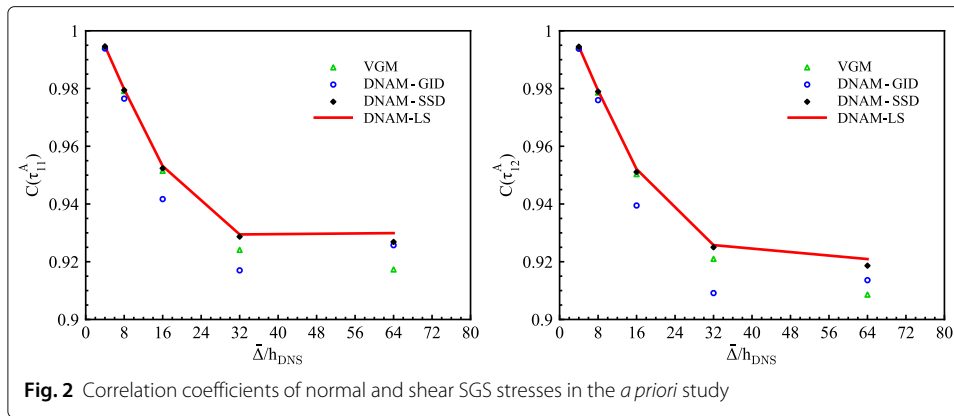
$$C(Q) = \frac{\langle (Q^{\text{real}} - \langle Q^{\text{real}} \rangle) (Q^{\text{model}} - \langle Q^{\text{model}} \rangle) \rangle}{\langle (Q^{\text{real}} - \langle Q^{\text{real}} \rangle)^2 \rangle^{1/2} \langle (Q^{\text{model}} - \langle Q^{\text{model}} \rangle)^2 \rangle^{1/2}}, \quad (37)$$

$$E_r(Q) = \frac{\langle (Q^{\text{real}} - Q^{\text{model}})^2 \rangle^{1/2}}{\langle (Q^{\text{real}})^2 \rangle^{1/2}}, \quad (38)$$

where $\langle \bullet \rangle$ represents the ensemble average of total samples. In the *a priori* study, we first investigate the impact of integrity basis tensors $\mathbb{T}_{ij}^{(n),A}$ on the SGS stress τ_{ij} by calculating the correlation coefficients at different filter widths, shown in Table 2. The normal components of the basis tensors $\mathbb{T}_{11}^{(n),A}$ share the similar correlation coefficients $C(\mathbb{T}_{ij}^{(n),A}, \tau_{ij}^A)$ with those of shear components $\mathbb{T}_{12}^{(n),A}$. The fourth term $\mathbb{T}_{ij}^{(4),A} = \bar{\mathbf{S}}\bar{\boldsymbol{\Omega}} - \bar{\boldsymbol{\Omega}}\bar{\mathbf{S}}$ contributes the highest correlation coefficients about 80% with the SGS stress, while the first term $\mathbb{T}_{ij}^{(1),A} = |\bar{\mathbf{S}}|\bar{\mathbf{S}}$ gives the worst predictions with correlation coefficients lower than 30% among these five basis tensors. It is worth noting that the terms $\mathbb{T}_{ij}^{(3),A} = (\bar{\boldsymbol{\Omega}}^2)^A$ and

Table 2 Correlation coefficients $C(\mathbb{T}_{ij}^{(n),A}, \tau_{ij}^A)$ with the increasing of the filter scales

$\bar{\Delta}/h_{\text{DNS}}$	$\mathbb{T}_{11}^{(1)}$	$\mathbb{T}_{11}^{(2)}$	$\mathbb{T}_{11}^{(3)}$	$\mathbb{T}_{11}^{(4)}$	$\mathbb{T}_{11}^{(5)}$	$\mathbb{T}_{12}^{(1)}$	$\mathbb{T}_{12}^{(2)}$	$\mathbb{T}_{12}^{(3)}$	$\mathbb{T}_{12}^{(4)}$	$\mathbb{T}_{12}^{(5)}$
2	0.227	0.44	0.518	0.824	0.549	0.219	0.429	0.513	0.819	0.545
4	0.227	0.425	0.519	0.821	0.534	0.221	0.415	0.514	0.816	0.529
8	0.233	0.401	0.513	0.808	0.509	0.228	0.394	0.509	0.804	0.5
16	0.256	0.384	0.498	0.789	0.488	0.253	0.38	0.498	0.781	0.468
32	0.3	0.385	0.487	0.777	0.491	0.306	0.389	0.493	0.755	0.448
64	0.334	0.398	0.498	0.788	0.535	0.384	0.431	0.508	0.737	0.464



$\mathbb{T}_{ij}^{(5),A} = (\bar{\mathbf{S}}^2 \bar{\boldsymbol{\Omega}} - \bar{\boldsymbol{\Omega}} \bar{\mathbf{S}}^2) / |\bar{\mathbf{S}}|$ have higher correlation coefficients with the SGS stress compared to the second term $\mathbb{T}_{ij}^{(2),A} = (\bar{\mathbf{S}}^2)^A$, therefore we keep all five basis tensors without any simplification in the paper. With the increasing of the filter widths, the correlation coefficients between the first basis tensor $\mathbb{T}_{ij}^{(1),A}$ and the SGS stress constantly increase, while those of the other four terms gradually drop but are still higher than those of the first term. These results indicate that the classical Smagorinsky model (linear relation with only the first basis tensor $\mathbb{T}_{ij}^{(1),A}$) cannot fully reconstruct the SGS stress.

Figures 2 and 3 respectively illustrate the correlation coefficients and relative errors of the normal and shear components of the SGS stress for different SGS models at a number of filter scales ranging from the inertial region to the dissipation range. Here, the VGM model is the velocity gradient model (see Eq. (14)) which has a high *a priori* accuracy among the classical SGS models. The DNAM-LS model is a DNAM model with *a priori* knowledge of DNS data, whose model coefficients are calculated by the least-squares method using the real SGS stress, namely $\sum_{m=1}^5 C_m \langle \mathbb{T}_{ij}^{(m),A} \mathbb{T}_{ij}^{(n),A} \rangle = \langle \tau_{ij}^A \mathbb{T}_{ij}^{(n),A} \rangle$, ($n = 1, 2, \dots, 5$). Here, $\mathbb{T}_{ij}^{(n)}$ represents the basis tensors displayed in Eq. (25). The model coefficients of the DNAM-GID model and DNAM-SSD model are calculated by the dynamic procedure based on conventional Germano identity (cf. Eq. (29)) and the newly proposed scale-similarity dynamic procedure (cf. Eq. (33)), respectively.

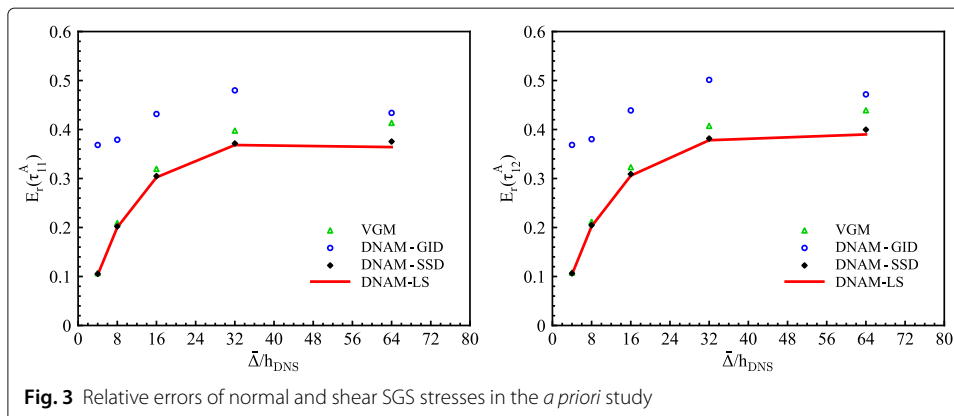


Table 3 Correlation coefficients and relative errors of the SGS stress at filter scale $\bar{\Delta} = 16h_{\text{DNS}}$ in the *a priori* study

	τ_{11}^A	τ_{22}^A	τ_{33}^A	τ_{12}^A	τ_{23}^A	τ_{13}^A
Model $\setminus C(\tau_{ij}^A)$						
DSM	0.256	0.255	0.24	0.26	0.279	0.253
DMM	0.628	0.617	0.605	0.608	0.624	0.615
VGM	0.952	0.949	0.949	0.947	0.95	0.95
ANNSGM-7-49	0.981	0.980	0.982	0.981	0.981	0.982
DNAM-LS	0.953	0.951	0.951	0.949	0.952	0.952
DNAM-GID	0.942	0.939	0.938	0.936	0.94	0.939
DNAM-SSD	0.952	0.95	0.95	0.948	0.951	0.951
Model $\setminus E_r(\tau_{ij}^A)$						
DSM	0.986	0.99	0.999	0.991	0.979	0.993
DMM	0.779	0.788	0.798	0.796	0.784	0.791
VGM	0.32	0.327	0.327	0.332	0.324	0.323
ANNSGM-7-49	0.199	0.201	0.202	0.197	0.194	0.192
DNAM-LS	0.302	0.309	0.31	0.314	0.307	0.306
DNAM-GID	0.432	0.438	0.442	0.446	0.44	0.439
DNAM-SSD	0.305	0.312	0.313	0.318	0.31	0.309

The DNAM-LS model has the highest correlation coefficients and the lowest relative errors with the SGS stress, since the DNS data are used to determine the model coefficients. The correlation coefficients and relative errors predicted by the proposed DNAM-SSD model are very close to the DNAM-LS model at all filter scales, which are much better than the DNAM-GID and VGM models. The DNAM-SSD model predicts the SGS stress accurately with the correlation coefficients overall higher than 92% and the relative errors less than 40% ranging from the viscous region to the inertial region. In contrast, the DNAM-GID model gives the worst prediction among these SGS models with the relative errors approximately over 40%. It is worth noting that the DNAM-SSD model performs better than the conventional VGM model at all filter widths, indicating that the basis tensors of the DNAM model are more complete than the velocity gradient in reconstructing the SGS stress.

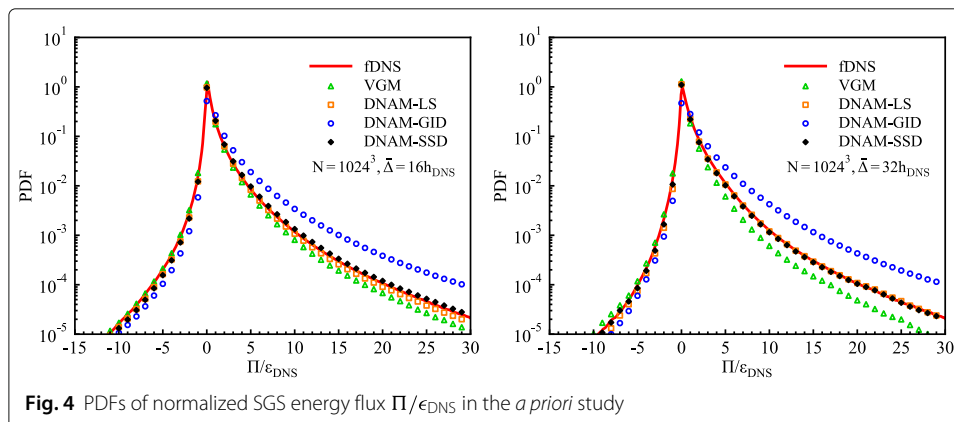
In order to further quantify the model accuracy of different SGS models in the *a priori* analysis, we compare the correlation coefficients and relative errors of the SGS stress at

Table 4 Correlation coefficients and relative errors of the SGS stress at filter scale $\bar{\Delta} = 32h_{\text{DNS}}$ in the *a priori* study

	τ_{11}^A	τ_{22}^A	τ_{33}^A	τ_{12}^A	τ_{23}^A	τ_{13}^A
Model $\setminus C(\tau_{ij}^A)$						
DSM	0.294	0.29	0.295	0.325	0.308	0.32
DMM	0.6	0.597	0.596	0.61	0.602	0.609
VGM	0.922	0.921	0.92	0.922	0.921	0.922
ANNSGM-7-49	0.944	0.945	0.944	0.944	0.943	0.942
DNAM-LS	0.927	0.926	0.925	0.927	0.926	0.927
DNAM-GID	0.913	0.913	0.912	0.913	0.913	0.914
DNAM-SSD	0.926	0.925	0.925	0.926	0.925	0.927
Model $\setminus E_r(\tau_{ij}^A)$						
DSM	0.975	0.978	0.977	0.963	0.971	0.964
DMM	0.802	0.804	0.806	0.797	0.803	0.797
VGM	0.405	0.407	0.409	0.405	0.407	0.404
ANNSGM-7-49	0.341	0.342	0.340	0.329	0.335	0.338
DNAM-LS	0.376	0.377	0.379	0.375	0.378	0.374
DNAM-GID	0.479	0.479	0.482	0.483	0.483	0.48
DNAM-SSD	0.38	0.381	0.383	0.379	0.382	0.378

filter widths $\bar{\Delta} = 16h_{\text{DNS}}$ and $32h_{\text{DNS}}$ listed in Tables 3 and 4, respectively. The DSM and DMM models use the Germano-identity dynamic procedure (see Eqs. (13), (17) and (18)) to dynamically determine model coefficients. The DNAM-SSD and DNAM-LS models give the best prediction of the SGS stress with correlation coefficients higher than 95% and 92% as well as relative errors lower than 30% and 38% at corresponding filter widths $\bar{\Delta} = 16h_{\text{DNS}}$ and $32h_{\text{DNS}}$ among these SGS models. In contrast, the DSM model performs the worst compared to other SGS models at both filter scales, whose correlation coefficients are lower than 30% and relative errors are nearly 100%. The DNAM-GID model predicts the SGS stress tangibly worse than the DNAM-SSD and DNAM-LS models, but is still much better than the classical DMM model with the consistent GID dynamic procedure. Besides, the performance of the VGM model in the *a priori* study is between the DNAM-GID model and DNAM-SSD model at both filter widths. We also compare the DNAM-SSD model with the artificial neural network-based spatial gradient models (ANN-SGM) proposed by Wang et al. [45] The ANNSGM-7-49 model consists of four fully-connected layers of neurons (4:20:20:49) and takes the integrity invariants as input to learn the model coefficients of the velocity gradient products for the neighboring seven-point stencil [45]. The DNAM-SSD model can accurately reconstruct the SGS stress with the similar accuracy to the ANN-based SGS model (ANNSGM-7-49) in the *a priori* analysis. These results demonstrate that the basis tensors of the DNAM model are more complete in modeling the SGS stress compared to those of the DMM model and VGM model. In the *a priori* analysis, the proposed scale-similarity dynamic procedure (SSD) shows distinct advantages over the conventional Germano-identity dynamic procedure (GID) in determining the model coefficients of SGS models.

Finally, we evaluate the SGS energy transfer for different SGS models by comparing the normalized SGS energy flux $\Pi/\epsilon_{\text{DNS}}$ shown in Fig. 4, where $\Pi = -\tau_{ij}\bar{S}_{ij}$ represents the SGS energy flux and ϵ_{DNS} denotes the dissipation rate calculated using the DNS data. The PDFs of the SGS energy flux reconstructed by the DNAM-SSD and DNAM-LS models coincide with the filtered DNS data at both filter scales $\bar{\Delta} = 16h_{\text{DNS}}$ and $32h_{\text{DNS}}$, which are obviously better than the VGM and DNAM-GID models. In comparison, the DNAM-GID model fails to predict the SGS energy transfer, indicating that the model-coefficient determination by the proposed SSD procedure is superior to that of the conventional GID procedure, and is well approximated to the DNAM-LS model in the *a priori* study.



7 A posteriori study of the DNAM models

The *a posteriori* testing of LES is important to illustrate the practical performance of the SGS models. In LES computations, the kinematic viscosity $\nu = 0.001$ is consistent with that of DNS. It is worth noting that an explicit filtering operation at the test-level filter scale is only introduced to determine the model coefficients, and no additional explicit filtering at the filter width $\bar{\Delta}$ is performed on the primary variables \bar{u}_i in the computations of LES. Two filter scales $\bar{\Delta} = 16h_{\text{DNS}}$ and $32h_{\text{DNS}}$ are selected to study the impact of filter widths on the SGS modeling. The newly proposed DNAM-SSD model is compared to the classical SGS models, including the implicit LES (ILES), the dynamic Smagorinsky model (DSM), the dynamic mixed model (DMM), the dynamic nonlinear algebraic model with conventional Germano-identity dynamic procedure (DNAM-GID) and the ANN-based SGS model (ANNSGM-7-49) [45]. It has been found that the filter-to-grid ratio $FGR = \bar{\Delta}/h_{\text{LES}} = 2$ can effectively reduce the influence of the spatial discretization errors on the SGS stress modeling [56–58]. Therefore, we fix the FGR value to 2 and the corresponding grid points of LES are $N = 128^3$ and 64^3 for the selected filter widths $\bar{\Delta} = 16h_{\text{DNS}}$ and $32h_{\text{DNS}}$. It is worth noting that both filter scales lie in the inertial range (cf. Fig. 1) and the scale-invariance assumption still holds, which are essential for the conventional dynamic models based on the Germano identity. The time step of LES is selected as $\Delta t_{\text{LES}} = 10\Delta t_{\text{DNS}}$ for all SGS models. The coarse-grained LES computations without any SGS models suffer from the numerical instability due to the nonlinear interactions between resolved large scales and residual scales. Implicit LES methods adopt the artificial dissipation to mimic the forward kinetic energy transfer from large scales to small scales. In this paper, we use the six-order compact-difference filtering scheme to provide necessary artificial dissipation for the numerical stability of coarse-grained LES computations, expressed as [59, 60]

$$\alpha_f \check{f}_{i-1} + \check{f}_i + \alpha_f \check{f}_{i+1} = \sum_{n=0}^3 \frac{a_n}{2} (f_{i+n} + f_{i-n}), \tag{39}$$

where a check “ $\check{\cdot}$ ” represents the dissipative filtering operation applied to the velocity field after each calculation of ILES, the parameter $0 < \alpha_f \leq 0.5$, and four coefficients a_n are determined by the Taylor-series expansion, namely [59, 60]

$$a_0 = \frac{11}{16} + \frac{5}{8}\alpha_f, \quad a_1 = \frac{15}{32} + \frac{17}{16}\alpha_f, \quad a_2 = \frac{-3}{16} + \frac{3}{8}\alpha_f, \quad a_3 = \frac{1}{32} - \frac{1}{16}\alpha_f. \tag{40}$$

In the paper, the control parameter $\alpha_f = 0.495$ is chosen for a commonly-used six-order low-dissipation filtering scheme [59, 60]. The pure scale-similarity type SGS model (DNAM-SSD) is numerically unstable due to lack of sufficient dissipation. Therefore, we couple the consistent compact-difference dissipative filtering scheme with the DNAM-SSD model to ensure the numerical stability of the LES calculations. For the ANNSGM-7-49 model, an artificial dissipation with the fourth-order hyperviscosity is introduced to maintain the numerical stability of the LES calculations [45]. The same instantaneous snapshot of the filtered DNS data is used as the initialization of the LES calculations for different SGS models. Table 5 summarizes the average computational time for the SGS stress modeling at both filter scales $\bar{\Delta} = 16h_{\text{DNS}}$ and $32h_{\text{DNS}}$. Compared to the classical DSM and DMM models, the DNAM model would not particularly increase too much computational cost: the modeling time of the DNAM-GID model is about 1.1 times that of the DMM model. The proposed SSD procedure simplifies the calculation process of the

Table 5 The computational cost of SGS stress modeling τ_{ij} for LES computations with the filter scales $\bar{\Delta} = 16h_{DNS}$ and $32h_{DNS}$

	DSM	DMM	DNAM-GID	DNAM-SSD
Model($\bar{\Delta} = 16h_{DNS}$)				
t(CPU·s)	5.9	9.941	10.996	5.989
t/t _{DMM}	0.593	1	1.106	0.603
Model($\bar{\Delta} = 32h_{DNS}$)				
t(CPU·s)	0.875	1.438	1.64	0.837
t/t _{DMM}	0.609	1	1.141	0.582

conventional GID method, which greatly reduces the computation costs and only takes about half the time of the DNAM-GID model (0.6 times that of the DMM model) at both filter widths $\bar{\Delta} = 16h_{DNS}$ and $32h_{DNS}$.

In the *a posteriori* testings of LES computations, we first compare the velocity spectra of different SGS models with those of the DNS and filtered DNS (fDNS) data at both filter scales $\bar{\Delta} = 16h_{DNS}$ and $32h_{DNS}$ shown in Figs. 5 and 6. LES of the incompressible turbulence is governed by the filtered Navier-Stokes equations (Eqs. (6) and (7)), therefore, the statistics of an ideal LES would be close to that of the fDNS data. The velocity spectra predicted by the ILES model are insufficiently dissipated and obviously higher than the fDNS data, while those modeled by the DSM and DMM models exhibit the tilde distribution due to excessive dissipation. The ILES generally reconstructs the inter-scale interactions and subgrid-scale effects by the artificial dissipation or dissipative spatial discretization schemes. Therefore, the ILES results are generally obtained without any explicit filtering operations [1–3]. Moreover, there is no filter width in ILES, and ILES results are very sensitive to the change of grid number. Statistics of ILES could converge to those of DNS when the grid is refined to the DNS level. For the DSM and DMM models, velocity spectra near the truncated wavenumbers are diminished by the model dissipation, resulting in the blockage of the kinetic energy cascade from large scales to small scales. Therefore the kinetic energy accumulates in the region of medium wavenumbers. The predicted velocity spectra of the DNAM-GID model are very similar to the DMM model, which has a significant deviation from the fDNS data. In contrast, the DNAM-SSD model outperforms the other SGS models and accurately reconstructs the velocity spectra at both filter scales $\bar{\Delta} = 16h_{DNS}$ and $32h_{DNS}$, which is very close to the ANNSGM-7-49 model. It is

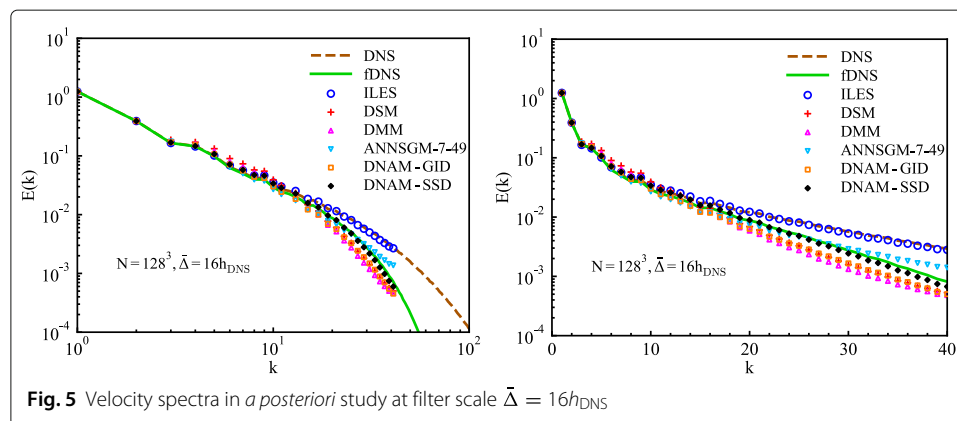
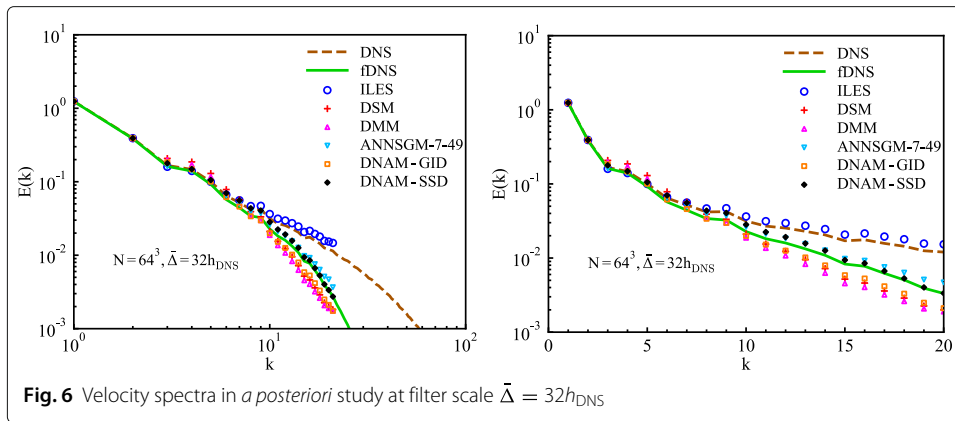


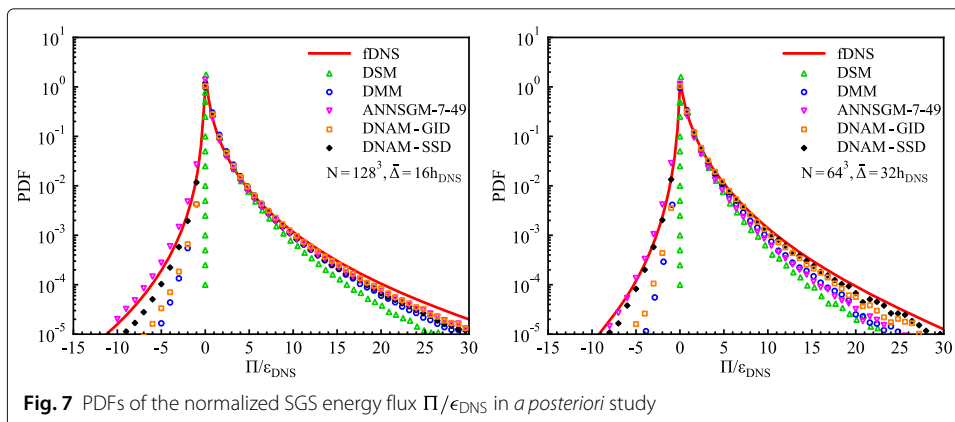
Fig. 5 Velocity spectra in a *a posteriori* study at filter scale $\bar{\Delta} = 16h_{DNS}$

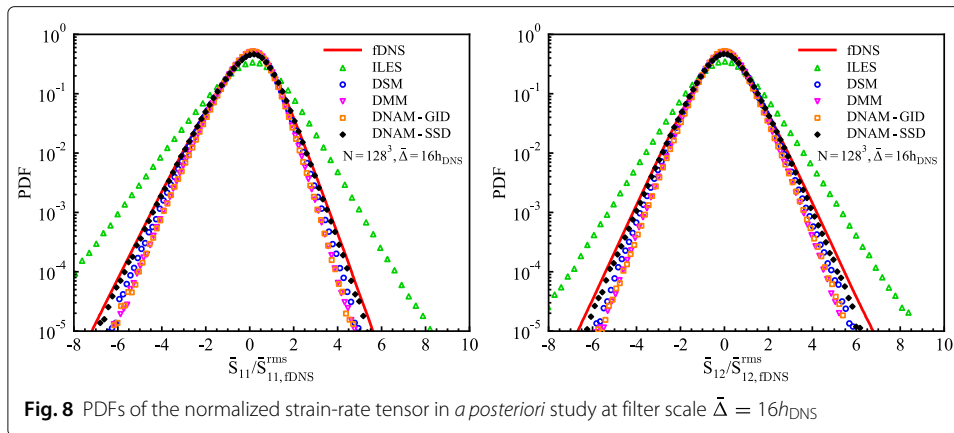


worth noting that the DNAM-SSD model does not require additional model training on the DNS data with *a priori* knowledge, compared to the ANN-based SGS models.

The SGS energy flux characterizes the kinetic energy transfer between the resolved large scales and the unclosed subgrid scales. The positive SGS energy flux stands for the forward energy cascade, while the negative SGS energy flux represents the energy backscatters. The PDFs of the normalized SGS energy flux Π/ϵ_{DNS} at filter scales $\bar{\Delta} = 16h_{DNS}$ and $32h_{DNS}$ are plotted in Fig. 7. In order to guarantee the numerical stability of the LES with the DSM model, the model coefficient C_S is restricted to be non-negative. The DSM model only reconstructs the forward SGS energy transfer whose modeled SGS energy flux is always non-negative. The PDFs of the SGS energy flux for the DMM and DNAM-GID models are obviously narrower than the fDNS data. In comparison, the DNAM-SSD model can accurately mimic both the forward SGS energy transfer and the energy backscatter, which is very similar to the ANN-based model (ANNSGM-7-49).

We further compare the normalized strain-rate tensor reconstructed by different SGS models, whose PDFs of the normal and shear components at both filter widths $\bar{\Delta} = 16h_{DNS}$ and $32h_{DNS}$ are illustrated in Figs. 8 and 9, respectively. In the figures, $\bar{s}_{ij,rms}^{fDNS} = \sqrt{\langle (\bar{s}_{ij}^{fDNS})^2 \rangle}$ represents the root-mean-square value of the strain-rate tensor calculated using the filtered DNS data shown in Table 6. The strain-rate tensor represents the local





straining of the turbulence flow. ILES overestimates the strain-rate tensor and the predicted PDFs of the strain rate are obviously wider than the fDNS data, while those PDFs predicted by the DSM, DMM and DNAM-GID models are apparently narrower due to the excessive model dissipation. In contrast, the DNAM-SSD model can recover more small scales and performs well on the predictions of the strain-rate tensor.

Figures 10 exhibits the PDFs of the normalized characteristic strain rate for different SGS models at filter scales $\bar{\Delta} = 16h_{DNS}$ and $32h_{DNS}$, where $|\bar{S}|_{fDNS}^{rms} = \sqrt{\langle (|\bar{S}|^{fDNS})^2 \rangle}$ stands for the root-mean-square value of the characteristic strain rate given from the filtered DNS data (see Table 6). ILES obviously fails to predict the characteristic strain rate, while the DSM, DMM and DNAM-GID models cannot well capture the peak of the PDFs in reconstructing the characteristic strain rate. In comparison, the PDFs of the characteristic strain rate predicted by the DNAM-SSD model are very close to the fDNS data.

We finally examine the reconstruction ability of the turbulent coherent structure by comparing the transient contours of the normalized vorticity, shown in Fig. 11. Here, the vorticity magnitude is normalized by the root-mean-square values calculated using the filtered DNS data: $\bar{\omega}_{fDNS}^{rms} = \sqrt{\langle \bar{\omega}_i^{fDNS} \bar{\omega}_i^{fDNS} \rangle}$ (see Table 6), where $\bar{\omega} = \nabla \times \bar{\mathbf{u}}$ denotes the resolved vorticity which is the curl of the resolved velocity field. The snapshots of LES calculations for different SGS models are selected on an arbitrary XY slice at the consistent

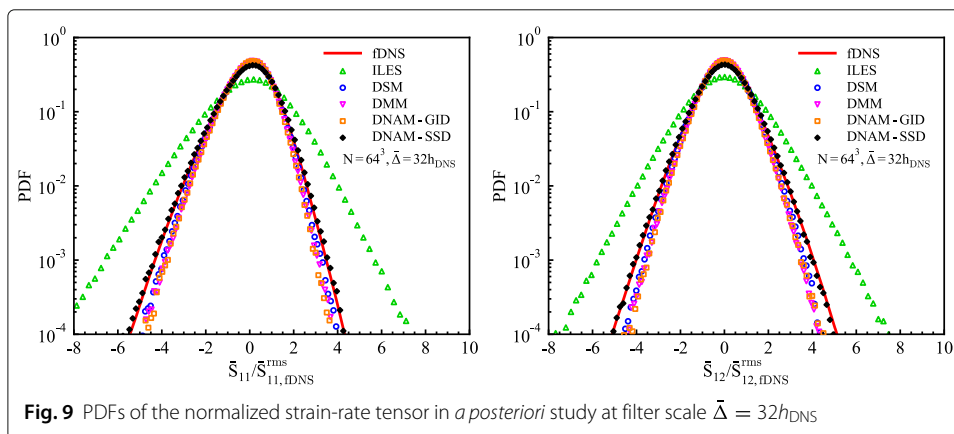


Table 6 The physical variables calculated using the filtered DNS data used for the variable normalization at the filter scales $\bar{\Delta} = 16h_{\text{DNS}}$ and $32h_{\text{DNS}}$

$\bar{\Delta}/h_{\text{DNS}}$	ϵ_{DNS}	$\bar{S}_{11,\text{fDNS}}^{\text{rms}}$	$\bar{S}_{12,\text{fDNS}}^{\text{rms}}$	$ \bar{S} _{\text{fDNS}}^{\text{rms}}$	$\bar{\omega}_{\text{fDNS}}^{\text{rms}}$
16	0.73	3.96	3.45	10.89	15.39
32	0.73	2.51	2.21	6.93	9.8

time with approximately two large-eddy turnover periods. For the DSM and DNAM-GID models, some small-scale flow structures are excessively dissipated and only large scales are maintained. Compared to the other SGS models, the vortex structures reconstructed by the DNAM-SSD model exhibit more similar spatial distribution to the fDNS data, and more multiple-scale flow structures are accurately recovered by the proposed DNAM-SSD model.

In order to test the impact of the explicit filters on the accuracy of the DNAM models, we choose two different types of explicit filters (the top-hat and differential Helmholtz filters). The top-hat filter in one dimension is expressed as [57, 61, 62]

$$\bar{f}_i = \frac{1}{2n} \left(f_{i-n/2} + 2 \sum_{j=i-n/2+1}^{i+n/2-1} f_j + f_{i+n/2} \right), \tag{41}$$

where $n = \bar{\Delta}/h_{\text{DNS}}$. The explicit form of differential Helmholtz filter is expressed as [63]

$$\bar{u}_i = (1 - \alpha^2 \nabla^2)^{-1} u_i = \left(1 - \alpha^2 \frac{\partial^2}{\partial x_k \partial x_k} \right)^{-1} u_i, \tag{42}$$

where $\alpha^2 = \bar{\Delta}^2/24$ [63]. The velocity spectra for different SGS models (ILES, DSM, DMM, DNAM-GID and DNAM-SSD) at the filter width $\bar{\Delta} = 16h_{\text{DNS}}$ with the top-hat and Helmholtz filters are displayed in Figs. 12 and 13, respectively. The LES results using both the top-hat and Helmholtz filters are very similar to those with the Gaussian filter (see Fig. 5). The ILES model exhibits insufficient dissipation, while the DSM, DMM and DNAM-GID models show bump distributions with excessive dissipation. In comparison, the DNAM-SSD model accurately predicts the velocity spectrum, which is almost coincident with the fDNS data. These results demonstrate that the accuracy of the DNAM models is not significantly affected by the type of the explicit filters.

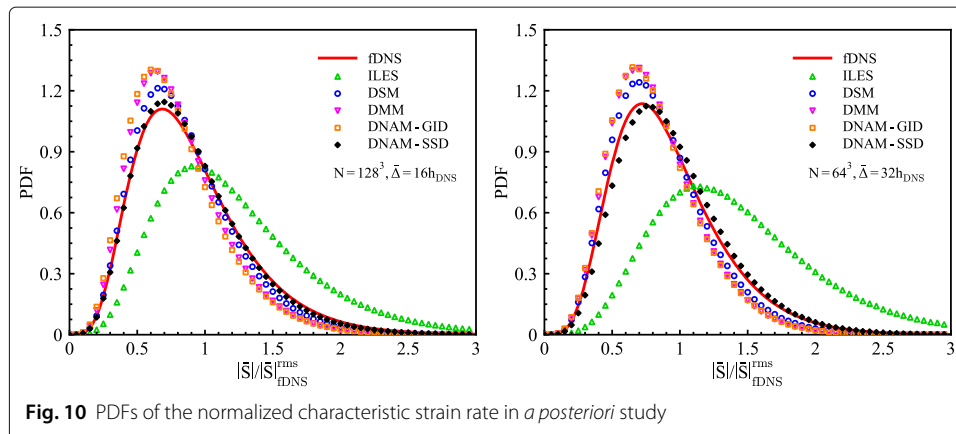
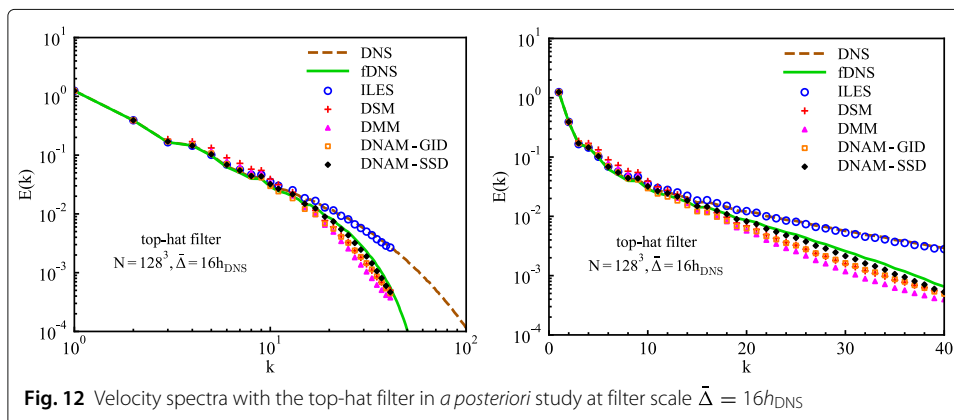
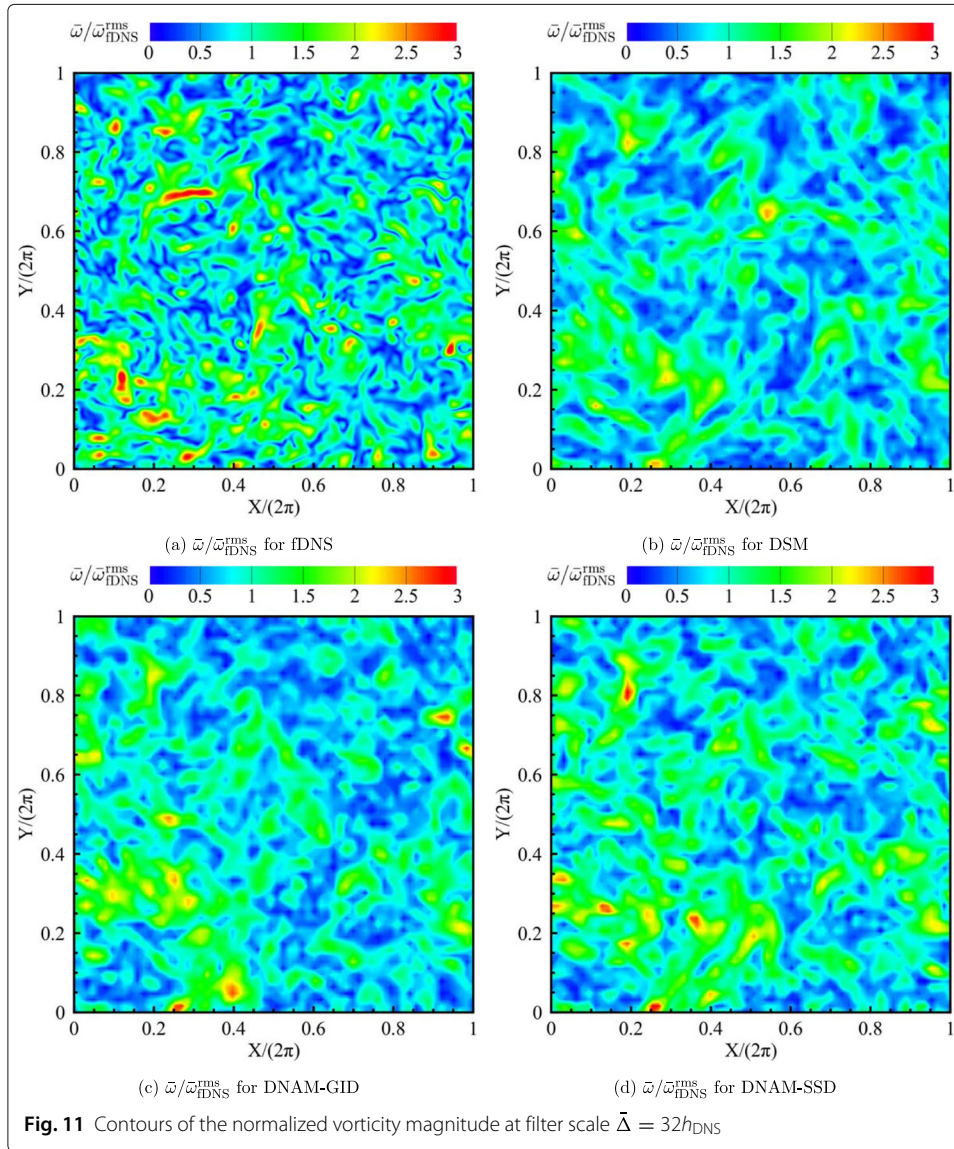


Fig. 10 PDFs of the normalized characteristic strain rate in *a posteriori* study



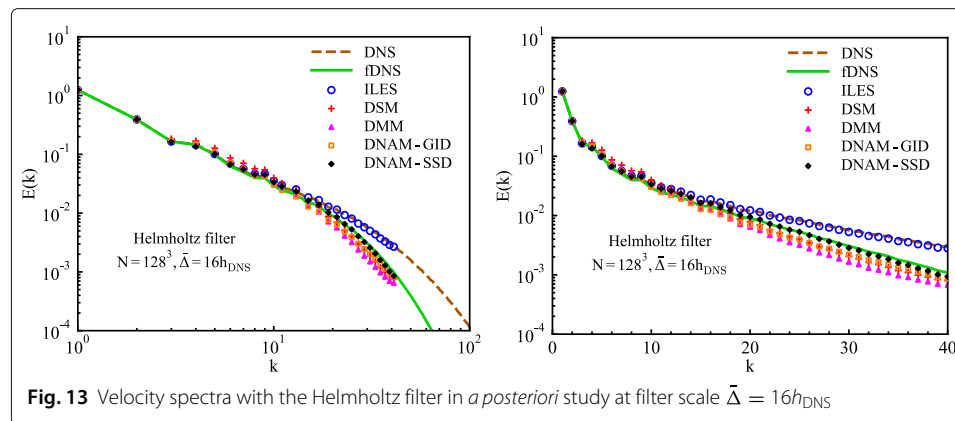


Fig. 13 Velocity spectra with the Helmholtz filter in a *posteriori* study at filter scale $\bar{\Delta} = 16h_{DNS}$

8 Conclusions

In the current work, we develop a dynamic nonlinear algebraic model with the newly proposed scale-similarity dynamic procedure (DNAM-SSD) for the large-eddy simulation of turbulence. In the DNAM-SSD model, the model coefficients are dynamically determined based on the scale-similarity relation, which greatly simplifies the conventional dynamic procedure based on the Germano identity (GID). The *a priori* analysis demonstrates that the proposed DNAM-SSD model outperforms the conventional velocity gradient model (VGM) and DNAM-GID model at a number of filter scales ranging from the inertial to dissipation ranges. The DNAM-SSD model gives the best prediction of the SGS stress with correlation coefficients higher than 95% and 92% as well as relative errors lower than 30% and 38% at corresponding filter scales $\bar{\Delta} = 16h_{DNS}$ and $32h_{DNS}$ in comparison with the dynamic Smagorinsky model (DSM), dynamic mixed model (DMM), VGM model and the DNAM-GID model, respectively. The proposed SSD procedure shows significant advantages over the conventional GID approach in determining the model coefficients of SGS models.

In the *a posteriori* testings of LES, the performance of the proposed DNAM-SSD model is examined at both filter widths $\bar{\Delta} = 16h_{DNS}$ and $32h_{DNS}$. The classical implicit-LES (ILES), DSM, DMM and DNAM-GID models are used for comparisons of the *a posteriori* model accuracy. ILES fails to predict the statistics of turbulence with insufficient dissipation, while the DSM and DMM models are over-dissipative, leading to the fact that small scales are diminished by the excessive dissipation. The results predicted by the DNAM-GID model are very similar to those of the DMM model and have obvious deviations from the filtered DNS data. In contrast, the predictions of the DNAM-SSD model are very close to the filtered DNS data in the velocity spectra, the statistics of SGS energy flux and strain rate, as well as the instantaneous spatial structures of the vorticity magnitude at both filter scales without increasing the computational cost. The modeling time of the DNAM-SSD model is only half the time of the DNAM-GID model (0.6 times that of the DMM model) at both filter widths. These results demonstrate that the current DNAM-SSD model is an effective framework for enhancing the advanced SGS stress modeling of LES.

Acknowledgements

This work was supported by Center for Computational Science and Engineering of Southern University of Science and Technology.

Authors' contributions

All authors read and approved the final manuscript.

Funding

This work was supported by the National Numerical Windtunnel Project (No. NNW2019ZT1-A04), by the National Natural Science Foundation of China (NSFC Grants No. 12172161, No. 91952104, No. 92052301, and No. 91752201), by the Shenzhen Science and Technology Program (Grants No. KQTD20180411143441009), by Key Special Project for Introduced Talents Team of Southern Marine Science and Engineering Guangdong Laboratory (Guangzhou) (Grant No. GML2019ZD0103), and by Department of Science and Technology of Guangdong Province (No. 2020B1212030001).

Availability of data and materials

The data that support the findings of this study are available from the corresponding author upon reasonable request.

Declarations

Competing interests

The authors declare that they have no competing interests.

Author details

¹Department of Mechanics and Aerospace Engineering, Southern University of Science and Technology, Shenzhen 518055 China. ²Southern Marine Science and Engineering Guangdong Laboratory (Guangzhou), Guangzhou 511458 China. ³Guangdong–Hong Kong–Macao Joint Laboratory for Data-Driven Fluid Mechanics and Engineering Applications, Southern University of Science and Technology, Shenzhen 518055 China. ⁴Department of Ocean Science, The Hong Kong University of Science and Technology, Hong Kong 999077 China.

Received: 14 November 2021 Accepted: 6 February 2022

Published online: 08 April 2022

References

1. Pope SB (2000) *Turbulent flows*. Cambridge University Press, Cambridge
2. Sagaut P (2006) *Large eddy simulation for incompressible flows: an introduction*, 3rd ed. Scientific computation. Springer, Berlin
3. Garnier E, Adams N, Sagaut P (2009) *Large eddy simulation for compressible flows*. Scientific computation. Springer, Dordrecht
4. Lesieur M, Metais O (1996) New trends in large-eddy simulations of turbulence. *Annu Rev Fluid Mech* 28(1):45–82
5. Meneveau C, Katz J (2000) Scale-invariance and turbulence models for large-eddy simulation. *Annu Rev Fluid Mech* 32(1):1–32
6. Durbin PA (2018) Some recent developments in turbulence closure modeling. *Annu Rev Fluid Mech* 50(1):77–103
7. Moser RD, Haering SW, Yalla GR (2021) Statistical properties of subgrid-scale turbulence models. *Annu Rev Fluid Mech* 53(1):255–286
8. Smagorinsky J (1963) General circulation experiments with the primitive equations: I. the basic experiment. *Mon Wea Rev* 91(3):99–164
9. Lilly DK (1967) The representation of small-scale turbulence in numerical simulation experiments. In: *Proceedings of IBM Scientific Computing Symposium on Environmental Sciences*, White Plains. Thomas J. Watson Research Center, Yorktown Heights. pp 195–210
10. Deardorff JW (1970) A numerical study of three-dimensional turbulent channel flow at large Reynolds numbers. *J Fluid Mech* 41(2):453–480
11. Clark RA, Ferziger JH, Reynolds WC (1979) Evaluation of subgrid-scale models using an accurately simulated turbulent flow. *J Fluid Mech* 91(01):1
12. Bardina J, Ferziger J, Reynolds W (1980) Improved subgrid-scale models for large-eddy simulation. In: *13th Fluid and Plasma Dynamics Conference*. American Institute of Aeronautics and Astronautics, Snowmass
13. Liu S, Meneveau C, Katz J (1994) On the properties of similarity subgrid-scale models as deduced from measurements in a turbulent jet. *J Fluid Mech* 275:83–119
14. Boris JP, Grinstein FF, Oran ES, Kolbe RL (1992) New insights into large eddy simulation. *Fluid Dyn Res* 10(4):199–228
15. Grinstein FF, Margolin LG, Rider WJ (2007) *Implicit Large eddy simulation: computing turbulent fluid dynamics*, vol. 113. Cambridge University Press, Cambridge
16. Xie C, Wang J, Li H, Wan M, Chen S (2018) A modified optimal LES model for highly compressible isotropic turbulence. *Phys Fluids* 30(6):065108
17. Chen S, Xia Z, Pei S, Wang J, Yang Y, Xiao Z, Shi Y (2012) Reynolds-stress-constrained large-eddy simulation of wall-bounded turbulent flows. *J. Fluid Mech.* 703:1–28
18. Sarghini F, de Felice G, Santini S (2003) Neural networks based subgrid scale modeling in large eddy simulations. *Comput Fluids* 32(1):97–108
19. Gamahara M, Hattori Y (2017) Searching for turbulence models by artificial neural network. *Phys Rev Fluids* 2(5):054604
20. Xie C, Wang J, Li K, Ma C (2019) Artificial neural network approach to large-eddy simulation of compressible isotropic turbulence. *Phys Rev E* 99(5):053113
21. Yuan Z, Xie C, Wang J (2020) Deconvolutional artificial neural network models for large eddy simulation of turbulence. *Phys Fluids* 32(11):115106
22. Yuan Z, Wang Y, Xie C, Wang J (2021) Dynamic iterative approximate deconvolution models for large-eddy simulation of turbulence. *Phys Fluids* 33(8):085125
23. Park J, Choi H (2021) Toward neural-network-based large eddy simulation: Application to turbulent channel flow. *J Fluid Mech* 914:16

24. Jiang C, Vinuesa R, Chen R, Mi J, Laima S, Li H (2021) An interpretable framework of data-driven turbulence modeling using deep neural networks. *Phys Fluids* 33(5):055133
25. Subel A, Chattopadhyay A, Guan Y, Hassanzadeh P (2021) Data-driven subgrid-scale modeling of forced Burgers turbulence using deep learning with generalization to higher Reynolds numbers via transfer learning. *Phys Fluids* 33(3):031702
26. Germano M, Piomelli U, Moin P, Cabot WH (1991) A dynamic subgrid-scale eddy viscosity model. *Phys Fluids A Fluid Dyn* 3(7):1760–1765
27. Lilly DK (1992) A proposed modification of the Germano subgrid-scale closure method. *Phys Fluids A Fluid Dyn* 4(3):633–635
28. Zang TA, Dahlburg RB, Dahlburg JP (1992) Direct and large-eddy simulations of three-dimensional compressible Navier-Stokes turbulence. *Phys Fluids A Fluid Dyn* 4(1):127–140
29. Vreman B, Geurts B, Kuerten H (1994) On the formulation of the dynamic mixed subgrid-scale model. *Phys Fluids* 6(12):4057–4059
30. Yu C, Xiao Z, Li X (2017) Scale-adaptive subgrid-scale modelling for large-eddy simulation of turbulent flows. *Phys Fluids* 29(3):035101
31. Zhou Z, Wang S, Yang X, Jin G (2020) A structural subgrid-scale model for the collision-related statistics of inertial particles in large-eddy simulations of isotropic turbulent flows. *Phys Fluids* 32(9):095103
32. Vreman B, Geurts B, Kuerten H (1997) Large-eddy simulation of the turbulent mixing layer. *J Fluid Mech* 339:357–390
33. Ghosal S, Lund TS, Moin P, Akselvoll K (1995) A dynamic localization model for large-eddy simulation of turbulent flows. *J Fluid Mech* 286:229–255
34. Pope SB (1975) A more general effective-viscosity hypothesis. *J Fluid Mech* 72(2):331–340
35. Lund TS, Novikov EA (1992) Parameterization of subgrid-scale stress by the velocity gradient tensor. In: Annual Research Briefs, Center for Turbulence Research, Stanford University, pp 27–43
36. Speziale CG (1991) Analytical methods for the development of reynolds-stress closures in turbulence. *Annu Rev Fluid Mech* 23(1):107–157
37. Gatski TB, Speziale CG (1993) On explicit algebraic stress models for complex turbulent flows. *J Fluid Mech* 254:59–78
38. Wong VC (1992) A proposed statistical-dynamic closure method for the linear or nonlinear subgrid-scale stresses. *Phys Fluids A Fluid Dyn* 4(5):1080–1082
39. Kosović B (1997) Subgrid-scale modelling for the large-eddy simulation of high-Reynolds-number boundary layers. *J Fluid Mech* 336:151–182
40. Wang B-C, Bergstrom DJ (2005) A dynamic nonlinear subgrid-scale stress model. *Phys Fluids* 17(3):035109
41. Wang B-C, Yee E, Bergstrom DJ, Iida O (2008) New dynamic subgrid-scale heat flux models for large-eddy simulation of thermal convection based on the general gradient diffusion hypothesis. *J Fluid Mech* 604:125–163
42. Marstorp L, Brethouwer G, Grundestam O, Johansson AV (2009) Explicit algebraic subgrid stress models with application to rotating channel flow. *J Fluid Mech* 639:403–432
43. Rasam A, Brethouwer G, Johansson AV (2014) A stochastic extension of the explicit algebraic subgrid-scale models. *Phys Fluids* 26(5):055113
44. Xie C, Yuan Z, Wang J (2020) Artificial neural network-based nonlinear algebraic models for large eddy simulation of turbulence. *Phys Fluids* 32(11):115101
45. Wang Y, Yuan Z, Xie C, Wang J (2021) Artificial neural network-based spatial gradient models for large-eddy simulation of turbulence. *AIP Adv* 11(5):055216
46. Wang Y, Yuan Z, Xie C, Wang J (2021) A dynamic spatial gradient model for the subgrid closure in large-eddy simulation of turbulence. *Phys Fluids* 33:075119
47. He G-W, Jin G, Zhao X (2009) Scale-similarity model for Lagrangian velocity correlations in isotropic and stationary turbulence. *Phys Rev E* 80(6):066313
48. Stallcup EW, Kshitiij A, Dahm WJ (2022) Adaptive scale-similar closure for large eddy simulations, part 1: subgrid stress closure. In: AIAA SCITECH 2022 Forum. American Institute of Aeronautics and Astronautics, San Diego
49. Stallcup EW, Dahm WJ (2022) Adaptive scale-similar closure for large eddy simulations, part 2: subgrid scalar flux closure. In: AIAA SCITECH 2022 Forum. American Institute of Aeronautics and Astronautics, San Diego
50. Wang J, Shi Y, Wang L-P, Xiao Z, He XT, Chen S (2012) Effect of compressibility on the small-scale structures in isotropic turbulence. *J Fluid Mech* 713:588–631
51. Wang J, Wan M, Chen S, Xie C, Zheng Q, Wang L-P, Chen S (2020) Effect of flow topology on the kinetic energy flux in compressible isotropic turbulence. *J Fluid Mech* 883:11
52. Shi Y, Xiao Z, Chen S (2008) Constrained subgrid-scale stress model for large eddy simulation. *Phys. Fluids* 20(1):011701
53. Chen S, Doolen GD, Kraichnan RH, She Z-S (1993) On statistical correlations between velocity increments and locally averaged dissipation in homogeneous turbulence. *Phys Fluids A Fluid Dyn* 5(2):458–463
54. Ishihara T, Kaneda Y, Yokokawa M, Itakura K, Uno A (2007) Small-scale statistics in high-resolution direct numerical simulation of turbulence: Reynolds number dependence of one-point velocity gradient statistics. *J Fluid Mech* 592:335–366
55. Ishihara T, Gotoh T, Kaneda Y (2009) Study of High-reynolds number isotropic turbulence by direct numerical simulation. *Annu Rev Fluid Mech* 41(1):165–180
56. Chow FK, Moin P (2003) A further study of numerical errors in large-eddy simulations. *J Comput Phys* 184(2):366–380
57. Xie C, Wang J, E W (2020) Modeling subgrid-scale forces by spatial artificial neural networks in large eddy simulation of turbulence. *Phys Rev Fluids* 5(5):054606
58. Yang XIA, Griffin KP (2021) Grid-point and time-step requirements for direct numerical simulation and large-eddy simulation. *Phys Fluids* 33(1):015108
59. Visbal MR, Gaitonde DV (2002) On the use of higher-order finite-difference schemes on curvilinear and deforming meshes. *J Comput Phys* 181(1):155–185
60. Visbal MR, Rizzetta DP (2002) Large-eddy simulation on curvilinear grids using compact differencing and filtering schemes. *J Fluids Eng* 124(4):836–847

61. Xie C, Wang J, Li H, Wan M, Chen S (2020) Spatial artificial neural network model for subgrid-scale stress and heat flux of compressible turbulence. *Theor App Mech Lett* 10(1):27–32
62. Xie C, Wang J, Li H, Wan M (2020) Spatially multi-scale artificial neural network model for large eddy simulation of compressible isotropic turbulence. *AIIP Adv* 10(1):015044
63. Bull JR, Jameson A (2016) Explicit filtering and exact reconstruction of the sub-filter stresses in large eddy simulation. *J Comput Phys* 306:117–136

Publisher's Note

Springer Nature remains neutral with regard to jurisdictional claims in published maps and institutional affiliations.

Ready to submit your research? Choose BMC and benefit from:

- fast, convenient online submission
- thorough peer review by experienced researchers in your field
- rapid publication on acceptance
- support for research data, including large and complex data types
- gold Open Access which fosters wider collaboration and increased citations
- maximum visibility for your research: over 100M website views per year

At BMC, research is always in progress.

Learn more biomedcentral.com/submissions

